OPTIMIZATION AND EXPERIMENTAL TESTS OF A CENTRIFUGAL TURBINE FOR AN OWC DEVICE EQUIPPED WITH A TWIN TURBINES CONFIGURATION

Laudino Rodríguez[a], Bruno Pereiras[b,*], Jesús Fernández-Oro[b] and Francisco Castro[c]

[a] (1) Integrated center of F.P. Maintenance and Production Services (C.I.F.P.M.S.P.)

Ciudad Tecnológica e Industrial Valnalón, Hornos Altos S/N, 33930, La Felguera, Spain

laudelinrg@gmail.com

[b] Department of Energy, University of Oviedo

Energy Building (EDZE), Campus de Viesques s/n, 33271, Gijón, Spain

* pereirasbruno@uniovi.es; jesusfo@uniovi.es

[c] Department of Energetic and Fluidmechanics Engineering. University of Valladolid

Paseo del Cauce 59, 47011, Valladolid, Spain

castro@eii.uva.es

*Corresponding author

ABSTRACT

The optimization of OWC devices has deserved much attention in the last few years. However, despite of this intense research activity, the most suitable turbine for OWC applications is still under debate. Recently, the twin-turbine configuration, where two unidirectional turbines are employed simultaneously, has emerged as a promising design. Although axial turbines are typically employed for those systems, the present paper demonstrates that the use of radial turbines can be also an interesting option.

In this work a radial geometry, specifically designed to be used in a twin-turbine configuration, has been manufactured at a reasonable cost for a lab-scale facility taking advantage of 3D printing technology. Encouraging preliminary results were obtained in an aerodynamic database of the turbine. In particular, the total-to-static efficiency under stationary conditions (i.e. at constant flow coefficients) reached remarkable high values. Hence, the performance curve of the turbine under such stationary conditions has been used to make an assessment of its non-stationary performance in order to compare this new radial turbine with respect to axial types available in the literature. The results revealed that radial turbines are clearly competitive against to axial ones when introduced in a twin-turbine configuration for OWC power plants.

Keywords: Wave energy, OWC, radial turbine, twin system, experimental.

NOMENCLATURE

$A_r=\pi\ b\ D_m$	Reference area	m^2	$u_R = D_m \cdot \omega/2$	Reference tangential velocity	m/s
b:	Blade Span	m	V_{AB}:	Tachogenerator terminal voltage	V
C_A:	Input coefficient		$v_R = Q/(\pi \cdot b \cdot D_m)$	Reference radial velocity	m/s
C_T:	Torque coefficient		W_{AB}:	Power in terminals of tachogenerator	W
D_{IN}:	Inlet diameter of turbine	m	W_{cu}:	Power loss caused by Joule heating	W
D_m:	Mean diameter of turbine	m	We:	Electric power	W
FEM:	Electromotive force	V	W_{FE}:	Iron losses	W
Hr	Relative humidity		W_{MEC}:	Mechanical losses	W
I:	Tachogenerator Intensity	A	$W_{IN}=\Delta Pt\text{-}_e\ v_R\ A_r$	Input power	W
l_b:	Chord blade	m	W_{OUT}:	Outlet power	W
K_v	Tachogenerator velocity constant	rd/V/s	Wr:	Resistant power	W
N:	Tachometer rotating speed	rd/s	Z:	Blades number	
P:	Barometric pressure	Pa	β_1, β_2:	Inner and outer blade angles	º
P_e:	Static pressure	Pa	$\Delta Pt\text{-}_e$:	Total to static pressure drop	Pa
P_{OWC}:	Pressure in OWC chamber	Pa	ΔP_e:	Static pressure drop	Pa
Q:	Flow rate	m^3/s	η	Turbine total-to-static efficiency	
Q_D:	Direct flow rate	m^3/s	$\overline{\eta}_{input}$:	Input efficiency	
Q_R:	Reverse flow rate	m^3/s	$\overline{\eta}_{system}$:	Efficiency of the whole system	
Q_T:	Total flow OWC chamber	m^3/s	$\overline{\eta}_{turbine}$	Net efficiency of the twin turbines	
R_1 , R_2:	Blade curvature		η_v	Volumetric efficiency	
R_{inner} , R_{outer}	Inner and outer rotor dimensions		θ_a	Air temperature	
Ri:	Tachogenerator internal resistance	Ω	ρ:	Air density	Kg/m^3
T:	Wave period	s	σ:	Rotor solidity	
T_o:	Total torque	N·m	ϕ:	Flow coefficient	
T_{oD}:	torque in direct mode	N·m	Φ_T:	Flow coefficient of the twin system	
T_{oR}:	torque in reverse mode	N·m	ω:	Angular velocity	rad/s

1. Introduction

Ocean's energy shows high potential for mid/long-future to make an important contribution to low-carbon electricity generation. Due to the technological barriers, only small facilities, mainly for research purposes, are operative at the present time, so a large amount of energy is still available for harnessing if those barriers are crossed. On the other hand, the marine environment is really challenging and very aggressive to the assembly and maintenance of ocean energy converters. In spite of this, different technologies to harvest these resources have been analysed in the last years [1,2], with the wave energy emerging as the most interesting option due to its high energy density [3], location possibilities (onshore, nearshore, offshore) and relative low environmental impact [4,5].

A wide number of patents for wave energy converters (WEC) has been registered in the last decades, proposing different alternatives for the exploitation of wave energy. [2,3,6]. In particular, the OWC device is probably the most widespread selection due to its installation possibilities and the less exposure to critical sea conditions [7].

The basic principle of an OWC device is the conversion of wave energy into pneumatic energy in a submerged chamber opened at the bottom to the incoming waves [7]. The waves produce an oscillatory movement of the water free surface, which is acting as a reciprocating piston so the air is alternatively discharged from the chamber to the atmosphere and then aspirated from the atmosphere towards the chamber. These processes, called exhalation and inhalation, take place sequentially according to the wave motion, generating a pulsating flow which can be used to drive an air turbine and thus generate electricity.

The main feature of OWC devices is the non-steady airflow conditions: the change of the airflow direction within every wave cycle as well as the oscillating variation of its magnitude. In particular, the wide range of instantaneous operating conditions is the key for the design of efficient turbines used as Power Take Off (PTO) for OWC devices. Early prototypes introduced non-return valves as the simplest solution to avoid changes in the airflow direction within the turbine, but their use was rapidly discouraged due to the high maintenance costs of their associated moving parts [8]. A recent proposal, though, has recovered its use for a new turbine equipped with a special non-return valve [9]. Another possibility considers the production of energy in both directions of the flow using bidirectional turbines. Hence, the valve system can be completely removed, despite of the severe penalty for the turbine overall efficiency. These bidirectional turbines are typically classified in two different families: Wells turbines [10,11] and impulse turbines [8]. They are broadly referenced in the literature concerning OWC devices: Wells turbines with or without guide vanes

and/or orientable blades and axial or radial impulse turbines also with or without guide vanes [7,8]. Nevertheless, the poor efficiencies of bidirectional turbines have led to the development of a relatively new concept: the twin turbine configuration (Figure 1), where two unidirectional turbines are assembled to the same rotating axis. In this arrangement, the turbines are alternating their role according to the pressure difference between the atmosphere and the OWC chamber: one of the turbines produces energy when the air is exhaled (Figure 1, left) , while the other has to drive power when the air is inhaled (Figure 1, right). Note that due to the absence of non-return valves, a special design is required for the turbines to prevent the reverse flow. At present time, numerical and experimental studies of twin-turbine systems have been carried out on axial turbines only [12–16]. Radial turbines, characterized by larger pressure differences [8,17], would be expected to perform better when working as a backflow preventer. However, there are hardly any studies [18] on the radial-flow turbine for twin systems.

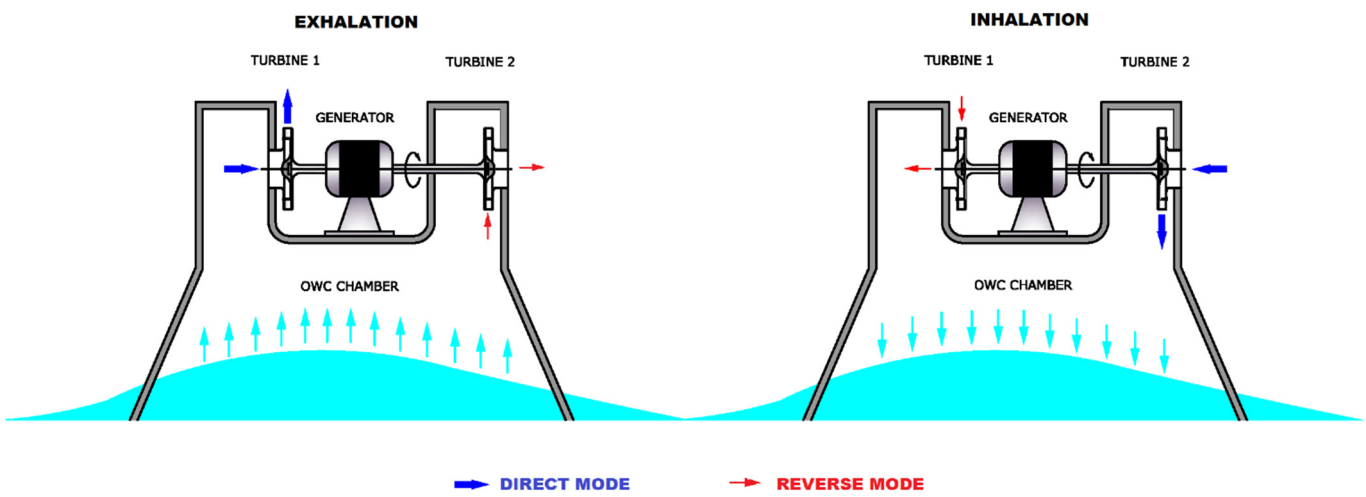

Figure 1 Twin turbines system layout

A preliminary evaluation of the performance of radial turbines for twin systems has been recently published by the authors [18] . The restrictions observed during the analysis of that initial design has led to the development and construction of a brand-new geometry which increases the turbine efficiency and strengthens its performance as backflow preventer. In this paper, the new geometry, the manufacturing process, the experimental rig and the testing procedure are presented. Additionally, the results from a test campaign in steady conditions are shown and a non-steady analysis based on such steady results is finally made in order to compare this new turbine to those available within the bibliography.

2. Dimensionless coefficients

In the literature [8], the performance of an OWC turbine in steady conditions is commonly assessed using the following non-dimensional coefficients:

$$\phi = \frac{v_R}{u_R} \qquad Eq.(1)$$

$$C_T = \frac{4\,T_o}{\rho\,(v_R^2+u_R^2)\,\pi\,b\,D_m^2} \qquad Eq.(2)$$

$$C_A = \frac{2\,W_{IN}}{\rho\,(v_R^2+u_R^2)\,\pi\,b\,D_m\,v_R} \qquad Eq.(3)$$

$$\eta = \frac{C_T}{C_A\,\phi} \qquad Eq.(4)$$

Being ϕ the flow coefficient, C_T, the torque coefficient, C_A the so-called input coefficient and η the total-to-static efficiency. The detailed definitions of the variables introduced in these coefficients are given in the nomenclature section.

On the other hand, the wave energy converter behaves non-steadily with typical time scales in the order of the waves period, so a temporal description of its relevant parameters is also needed. Fortunately, the time scales within the turbine stages (i.e., the blade passing frequencies) are two or three orders of magnitude lower than the global fluctuations in the OWC system (the incoming waves at the boundaries), so it can be perfectly assumed that the turbine works under quasi-steady boundary conditions in regard to the wave time scales [15,19]. This means that the steady characterization of the turbine can be used as input data to perform a further non-steady analysis of the whole system, where the input variable is the manometric static pressure inside the chamber defined according to a sinusoidal evolution as:

$$P_{OWC} = P_{max}\,sin(\frac{2\pi t}{T}) \qquad Eq.(5)$$

Where P_{max} is the maximum pressure at the OWC within a cycle, *T is* the period of the oscillation and *t* is the current time.

During operation, both turbines of the twin system are exposed to the same pressure difference. Their performance is switched from direct to reverse mode and vice versa according to the sign of the pressure difference. Hence, the total outgoing flow rate transferred from the chamber is the combination of both direct (Q_D) and reverse (Q_R) mode flowrates:

$$Q_T = Q_D + Q_R \qquad Eq.(6)$$

So, the volumetric efficiency of the OWC can be determined as the ratio between those direct and the total flow rates, according to:

$$\eta_V = \frac{Q_D}{Q_T} = \frac{Q_D}{Q_D + Q_R} \qquad Eq.(7)$$

However, the turbine efficiency is also relevant, so it must be evaluated in combination with the efficiency of the twin system. This can be assessed according to the following expression:

$$\bar{\eta}_{system} = \frac{\frac{1}{T}\int_0^T \omega\, T_o\, dt}{\frac{1}{T}\int_0^T \Delta P_{t-e}\, Q_T\, dt} = \underbrace{\frac{\frac{1}{T}\int_0^T \Delta P_{t-e}\, Q_D\, dt}{\frac{1}{T}\int_0^T \Delta P_{t-e}\, Q_T\, dt}}_{\bar{\eta}_{input}} \underbrace{\frac{\frac{1}{T}\int_0^T \omega\, (T_{oD} - T_{oR}) dt}{\frac{1}{T}\int_0^T \Delta P_{t-e}\, Q_D\, dt}}_{\bar{\eta}_{turbine}} \qquad Eq.(8)$$

Or more compactly:

$$\bar{\eta}_{system} = \bar{\eta}_{input}\, \bar{\eta}_{turbine} \qquad Eq.(9)$$

Note that the so-called input efficiency, $\bar{\eta}_{input}$ is related to the volumetric efficiency (η_V) of the OWC chamber, but in terms of power instead of flow rates only; and that the turbine efficiency, $\bar{\eta}_{turbinne}$ is the net efficiency of the twin turbines, considering the resistant torque (T_{oR}) produced in the reverse mode.

Alternatively, the system flow coefficient is also defined as the ratio between the mean flow velocity of both turbines and the reference tangential velocity in the turbine mean diameter of the turbine:

$$\Phi_T = \frac{Q_T}{\pi\, D_m\, b\, u_R} \qquad Eq.(10)$$

Where Q_T is the total flow rate, D_m is the mean diameter of turbine, b is the blade span and u_R is the reference tangential velocity at midspan.

Note that the performance under non-steady conditions can be better addressed using more complex techniques like stochastic methods, spectral models or time-domain analysis. However, the application of such models to non-linear turbines is out of the scope of this paper. In any case, the method applied in this work, widely used in the bibliography, provides relevant information to compare turbines in terms of maximum efficiencies.

3. Geometry optimization

To enhance the performance of a radial turbine for the twin-system configuration, a geometry optimization has been firstly completed, taking advantage of a previous CFD analysis [18]. Although more details can be found in [18], some comments on the CFD model are shown here. The CFD geometry of the turbine was created at the same scale as the experimental geometries thus the Reynolds number, defined as $Re=\rho\, v_R$

D_m / μ, reaches a value of 2.6e5. Considering that value above the critical Reynolds number agrees, in spite of being different geometries, with numbers given in [20,21] for both inflow radial turbines and axial impulse turbines.

The CFD geometry is composed of three main parts: elbow, rotor and diffuser, was initially designed to work with a centrifugal flow (or “direct mode” operation, from now on). Figure 2 shows a 3D view of the model (a single passage with circumferential periodicity) and the corresponding boundary conditions.

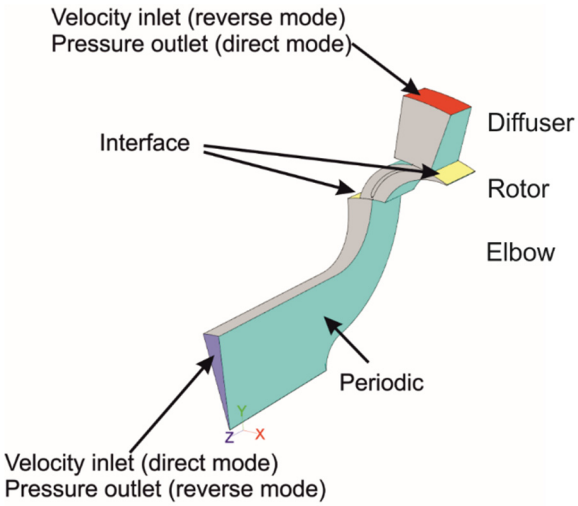

Figure 2. Geometry and boundary conditions of the CFD model

When this turbine, installed in the twin configuration, is to be operated in the centripetal direction (or “reverse mode”), it is extremely important that the turbine could perform as an optimal backflow preventer to maximize the overall efficiency of the system. Thus, a design criterion can be declared as the larger the input coefficient in reverse mode, the better performance as backflow preventer.

In [18] it was revealed that this kind of radial turbine shows several strong points, making it suitable for working in a twin turbines configuration. Nevertheless, some penalties were also observed after analysing the results in the first numerical model, mainly related to a weak performance when working in reverse mode as a backflow preventer (1) and an excessive kinetic energy loss at the diffuser in direct mode (2).

Consequently, for this investigation, a re-design of the original geometry has been carried out to include some new modifications in the turbine and correct all those detrimental problems. In particular:

a) To improve the performance as a backflow preventer in reverse mode:

The suppression of three structural ribs, originally introduced for rigidity, in the connection of the shroud at the elbow (Figure 3), which were acting as guide vanes during the reverse mode, breaking

the swirl generated rotor downstream, and thus reducing the (desirable) loss at the elbow. A complementary CFD model of the single elbow (with and without ribs) demonstrates the significant improvement of the unribbed elbow with higher losses helping to strengthen the performance as a backflow preventer (Figure 4), and enhance the twin system efficiency. Therefore, any guide vanes/ribs were suppressed in order to optimize the performance as a backflow preventer in the reverse mode. Overcoming this issue forced a change in the mechanical design of the turbine (see Figure 7 afterwards) with respect to that shown in [18].

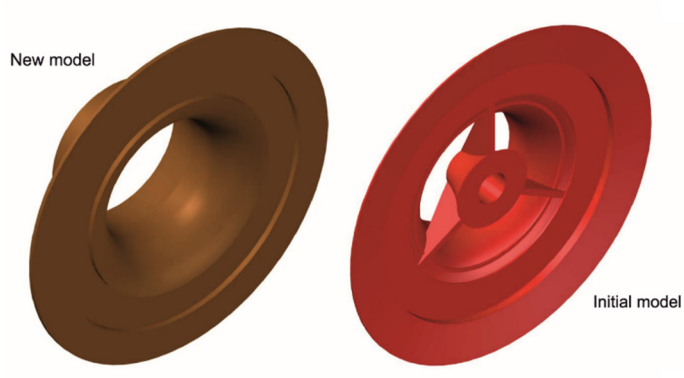

Figure 3. Connection of the shroud at the elbow.

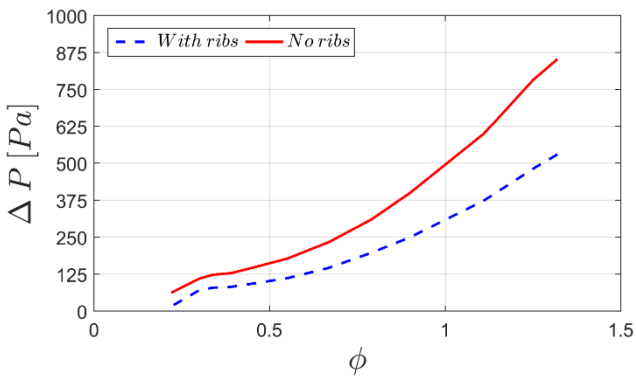

Figure 4. Effect of the structural ribs in the elbow loss during reverse mode.

b) To reduce the kinetic energy loss at the outlet in direct mode

One of the most remarkable problem of the original geometry was the large difference between the total-to-total and the total-to-static efficiency when working in direct mode. After an initial reconsideration of the diffuser, the in-depth analysis of the numerical results redirected the attention towards the rotor outlet.

Therefore, in order to obtain a real reduction of the kinetic energy at the outlet, actions were taken on the rotor, focusing on the blade profile and the rotor solidity. In the original geometry the outer angle (β_2, Figure 5) of the blade was fixed to 5 degrees, resulting in very closely spaced blades, a very reduced outlet section and a really high velocity magnitude at the outlet. Several CFD simulations were then conducted for various blade profiles equipped with different β_2 while maintaining the inlet angle (β_1) to 65 degrees, aiming to find the optimal β_2 for this application. Note that, since the kinetic energy was affecting the performance of the direct mode, simulations were carried out in the centrifugal direction only, using the rotor efficiency as the relevant parameter for the optimization.

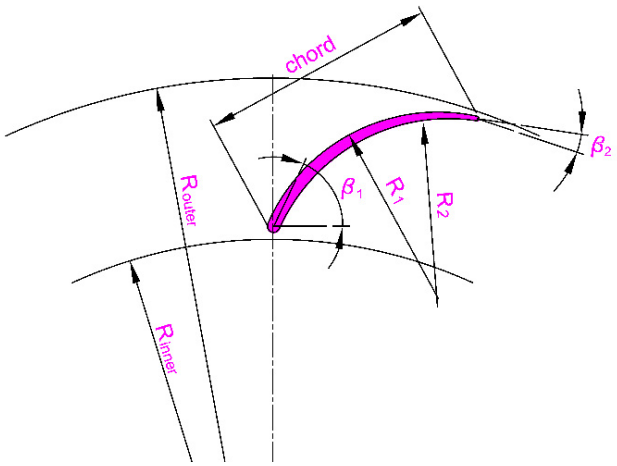

Figure 5. Blade profile.

The increment of the maximum efficiency obtained with the modified blade profile with respect to the original airfoil is shown as a function of the blade external angle (β_2) in Table 1. A parabolic fitting was finally used to determine the optimum blade angle, corresponding to 11 degrees.

Table 1. Efficiency gain in direct mode vs blade external angle.

β_2 [º]	5	9	13	15
$\eta_{max}/\eta_{max}^{ref}$	0.00	0.07	0.10	0.06

Alternatively, it was also found that the rotor solidity plays a major role in the turbine performance. Furthermore, not only presents a relevant impact on the efficiency in the direct mode, but it is also crucial

in the performance of the turbine as a backflow preventer during the reverse mode. To quantify that influence, several simulations were additionally carried out for different rotor solidities, 1.83, 2.20 and 2.75, which correspond to 20, 24 and 30 blades respectively. The rotor solidity was defined as:

$$\sigma = \frac{l_B\, Z}{\pi\, D_m} \qquad Eq.(11)$$

Where l_B is the blade chord, Z is the number of blades and D_m is the rotor mean diameter.

The results, shown in Figure 6, reveal that the overall efficiency $\bar{\eta}_{system}$ is quite similar for the whole set of cases. Actually, since there are many effects involved, some comments are needed at this point. It has been confirmed that increasing the solidity improves the guidance of the flow and lead to gain efficiency in direct mode in spite of having larger velocities at the rotor outlet due to the finite thickness of the blades. In addition, the performance as a backflow preventer is also affected because larger solidities reduce the vorticity at the elbow in reverse mode reducing the $\bar{\eta}_{input}$. Both effects compensate each other to show no clear difference in the $\bar{\eta}_{system}$. The real effect of the solidity on the $\bar{\eta}_{system}$ is that the flow coefficient Φ_T corresponding to maximum $\bar{\eta}_{system}$ is shifted towards lower values as solidity increases.

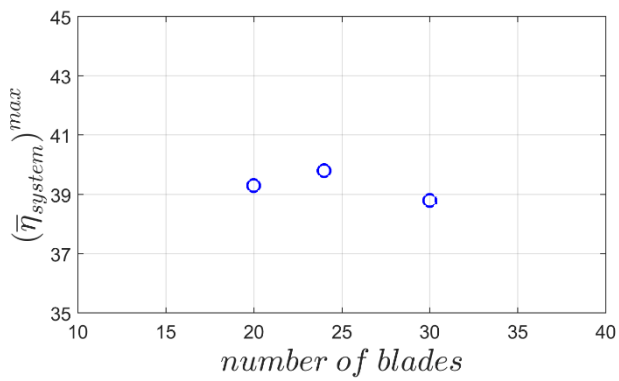

Figure 6. Influence of the rotor solidity on the twin system efficiency.

Considering these results, the intermediate solution was adopted for the new design, using 24 blades with the following characteristics.

Table 2. Main dimensions [mm] of the new and previous blades

	Chord	*R_1 ; R_2*	*R_{inner}*	*R_{outer}*	*β_1 [º]*	*β_2 [º]*
New blade	*43.2*	*28.8 ; 28.8*	*75*	*100*	*65*	*11*
Previous blade	*50.4*	*28 ; 29*	*75*	*99.2*	*65*	*5*

4. Turbine mechanical design and experimental rig

The final concept of the manufactured geometry is shown in Figure 7, where the whole set of elements that compose the turbine are exploded. The number of moving parts has been minimized to simplify operation and reduce maintenance costs. Rotating parts (2, 3, 9 and 10) are mounted on the shaft (5) which is supported by a ball bearing (7). The whole set of moving parts, including the diffuser as well, is fixed by one single nut (8). The inlet connection (1), separated from the rest of the components, is assembled coaxially with the rest.

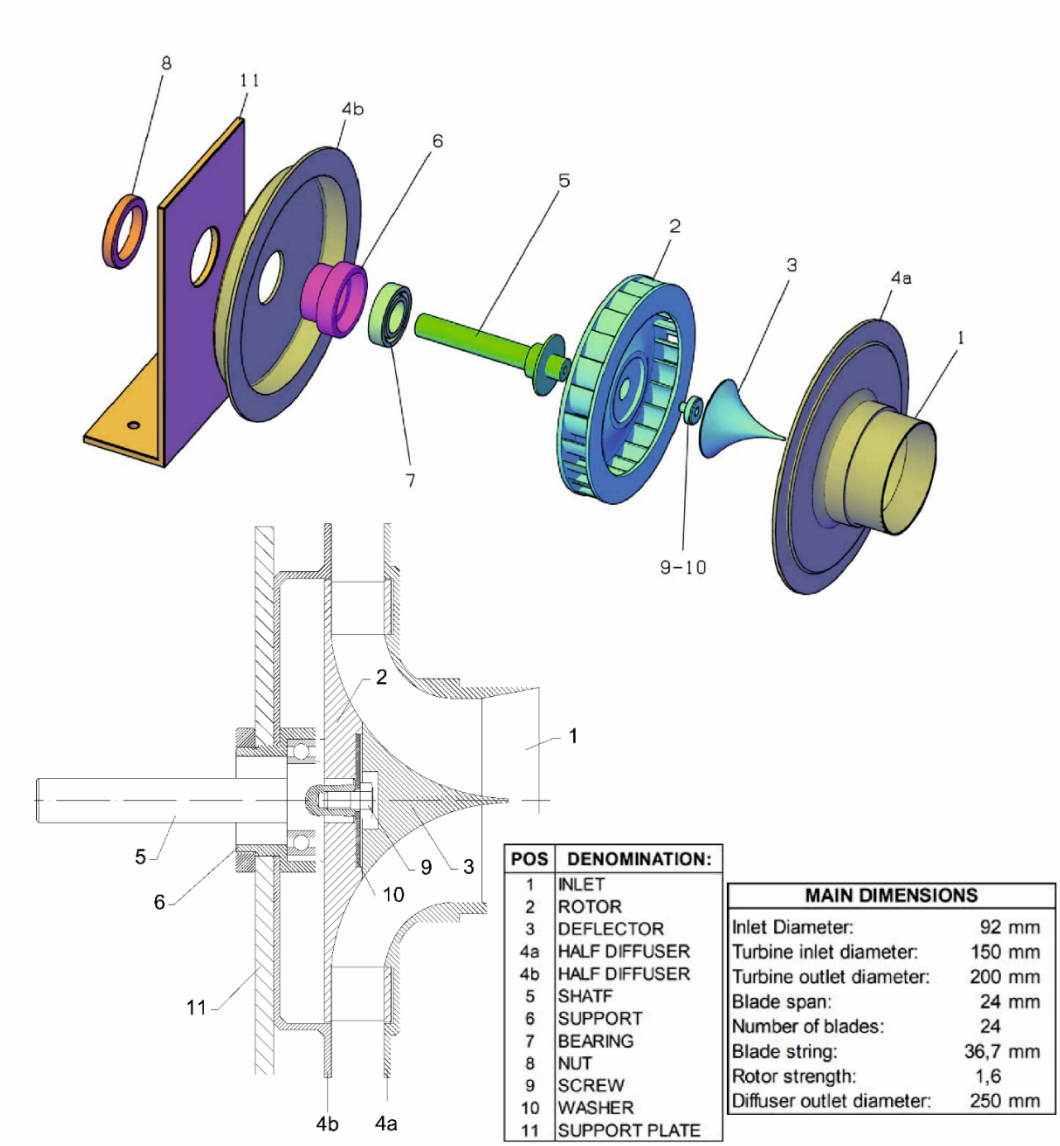

POS	DENOMINATION:
1	INLET
2	ROTOR
3	DEFLECTOR
4a	HALF DIFFUSER
4b	HALF DIFFUSER
5	SHATF
6	SUPPORT
7	BEARING
8	NUT
9	SCREW
10	WASHER
11	SUPPORT PLATE

MAIN DIMENSIONS	
Inlet Diameter:	92 mm
Turbine inlet diameter:	150 mm
Turbine outlet diameter:	200 mm
Blade span:	24 mm
Number of blades:	24
Blade string:	36,7 mm
Rotor strength:	1,6
Diffuser outlet diameter:	250 mm

Figure 7. Top: Exploded view of the turbine assembly. Bottom: Side view of the turbine assembled and identifying numbers.

The geometrical dimensions of the turbine main components are referred at the bottom of Figure 7. Most of the non-commercial components (1, 2, 3, 4a, 4b) have been designed with the help of CAD software and built in a 3D printer model Witbox (manufacturer BQ). Precisely, the turbine has been printed taking advantage of the whole printer capacity of 297x210x200 mm (length x width x height) and the maximum print quality: 50 microns. Under these conditions, the printer spent 57 hours to complete the whole assembly using PLA (biodegradable polylactic acid) as the building material. The shaft (5), the bearing support (6) and the nuts (8) have been manufactured in aluminum, using a conventional machine-tool while the support plate (11) is made of steel. The bearing, the screw and the washer are standard commercial elements.

The upper Figure 8 shows the elements 1, 2, 3 and 4 built with 3D printer, while the bottom Figure 8 shows the turbine assembly on the test bench.

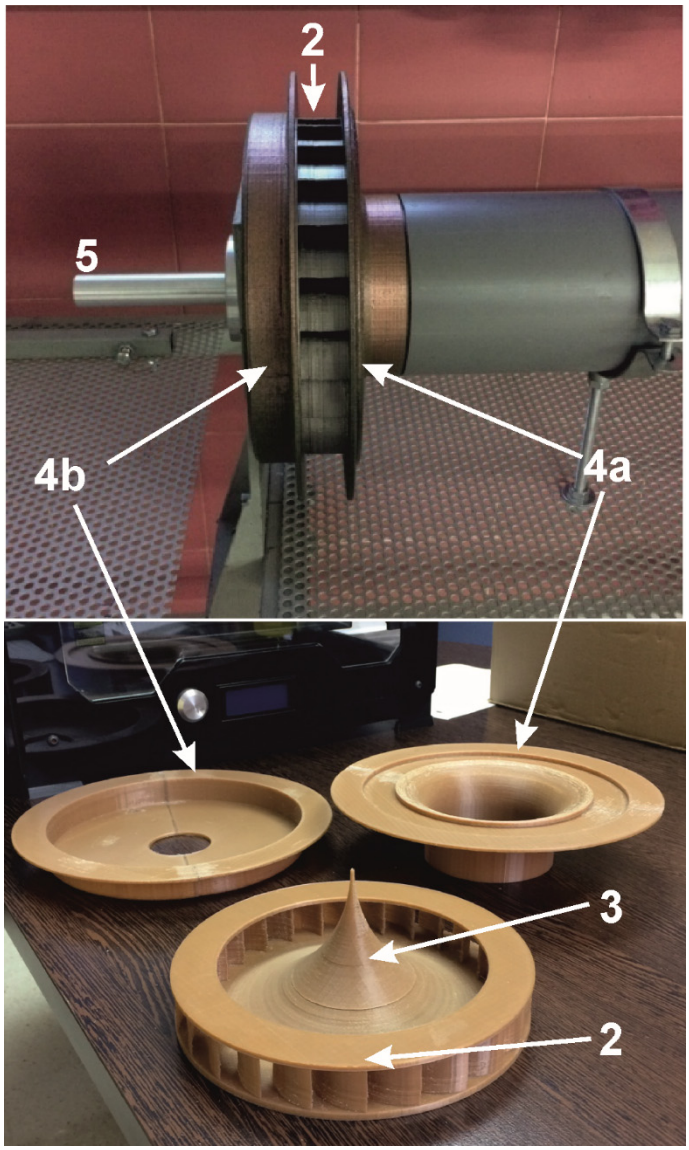

Figure 8. Top: Turbine assembled. Bottom: components built with the 3D printer. Labels in Figure 7.

A sketch of the setup is shown in Figure 9. The whole rig, mounted on a steel structure, is made of PVC tubes (3-6) with 103 mm in diameter. The air flow is supplied by a centrifugal fan (2) connected to a frequency inverter (15) in order to obtain variable flow rates. According to the manufacturer data the fan provides a maximum flow rate of 1250 m^3/h (free exit) and maximum static pressure (at zero flow rate) of 1600 Pa. The flow rate is measured with a Venturimeter (5) using a testo 435/9 (9) differential pressure sensor. To reduce turbulence levels and assure an inlet unidirectional velocity, a honeycomb is also installed between the centrifugal fan and the Venturimeter.

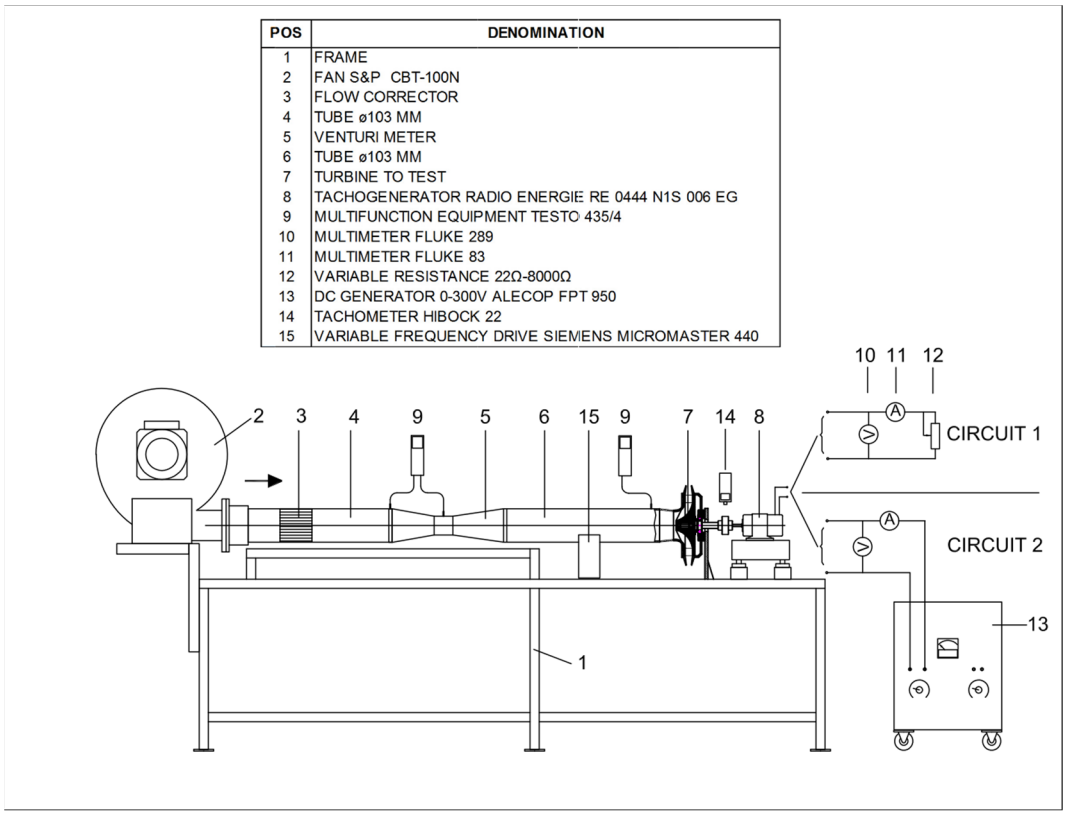

Figure 9. Experimental set up.

The experimental tests were carried out with a tachogenerator (8) running as a generator or a motor depending on the test to be made. To perform as a generator, the tachogenerator was connected to a grid of resistors using circuit no.1 (Figure 9) so the power generated by the turbine (7) could be dissipated for a variable range of loads (from 22 to 80 kΩ). When the tachogenerator is required to run as a motor it is connected to a DC power supply (13) using circuit no 2. In this case, the required rotational speed is obtained modifying the voltage of the DC power supply.

Additional measuring devices are both Fluke 83 and 289 multimeters (10 and 11) that provide the measurements of voltage and current respectively. Besides, the torque and the rotating speed of the turbine were given by the tachogenerator (8) whose basic characteristics are shown in Table 3. Note that in the case of free rotation tests (i.e., the tachogenerator is disconnected), the rotating speed is measured with an optical tachometer (14), model Hibock 22.

Table 3. Tachogenerator specifications

Maker:	Predilec Radio Energie
Ref:	RE 0444 N1S 006 EG
ωmax:	10000 rpm
Vmax:	600 V
K_v:	1.754 rd/V/s
Ri:	100 Ω
Imax:	0.180 A
Wmax:	108 W

Finally, the atmospheric pressure, temperature and humidity are measured with a Weather station DAVIS VANTAGE VUE 6351 and multifunction Testo 435/4 in order to calculate the air density. Details of the accuracy of measurement equipment are shown in the Table 4.

Table 4. Accuracy of measurement equipment

ACCURACY OF MEASUREMENT EQUIPMENT				
Magnitude	Symbol	Measurement equipment	Minimum accuracy	
Barometric pressure	P	Station DAVIS VANTAGE VUE 6351	±100	Pa
Room temperature	t	Testo 435/4	±0.3	ºC
Relative humidity	Hr	Testo 435/4	±2	%
Static pressure inlet turbine	Pe	Testo 435/4	±2	Pa
Differential pressure in Venturi	ΔPe	Testo 435/4	±2	Pa
Angular velocity	N	Tachometer Hibok 22	±0.15	rpm

Voltage DC	V	Multimeter Fluke 83	±(0.1%+0.1)	V
Intensity DC	I	Multimeter Fluke 289	±(0.15%+0.02)	mA
Resistance DC	R	Multimeter Fluke 83	±(0.4%+0.1)	Ω
Tachogenerator terminal voltage	V_{TD}	Tachogenerator RE 0444 N1S 006 EG	±1	%

The impact of the uncertainty of those measuring devices towards the accuracy of the complete measuring chain has been estimated using Klein's theory on uncertainty transmission [22]. Hence, the turbine performance is complemented with the expected uncertainties in every working point of the steady experimental tests, as it will be shown later in Figure 12 and Figure 13.

5. Experimental procedure and results

The performance curves of the turbine under steady conditions for both direct and reverse modes have been obtained experimentally. For that purpose, it was necessary to conduct different types of tests in order to address the contribution of friction losses. In particular, the following tests are described in this section.

a) A tachogenerator loss test (in order to determine mechanical/electrical loss of the tachogenerator)
b) A turbine + tachogenerator loss test (in order to determine mechanical loss of the turbine)
c) Both turbine tests in direct mode (centrifugal) and reverse mode (centripetal) to determine the turbine performance

Table 5 summarizes all the measured variables and how they are obtained with the available equipment.

Table 5. List of measured variables and their provenance.

	Magnitude	Variable	Geometric	Measured	Calculated	Equipment
Dimensionless coefficients Φ, C_T, C_A	u_R	D_m	x			
		ω		x		Tachogenerator (8) Tachometer (14)
	v_R	Q			x	Venturi (5),Testo 435 (9)
		D_m , b	x			
	To				x	Tachogenerator (8) Tachometer (14)
	ΔP_e , θ_a , H_r , P			x		Testo 435 (9)
	ρ	θ_a, H_r, P			x	Weather Station

5.1. Tachogenerator loss test

This first test is performed to measure, for different rotating speeds, the voltage and current consumed by the unloaded tachogenerator when running as a motor, for different rotating speeds. The voltage applied to the terminals of the tachogenerator is ranged between 0 and 85 V DC and the resulting intensities are recorded to be processed according to the theory of electric machines, as follows:

$$W_{AB} = V_{AB}\, I \qquad Eq.(12)$$

$$W_{CU} = R_i\, I^2 \qquad Eq.(13)$$

$$W_{FE} + W_{MEC} = W_{AB} - W_{CU} \qquad Eq.(14)$$

$$N = \frac{V_{AB} - R_i\, I}{1/K_v} \qquad Eq.(15)$$

Where V_{AB} is the voltage applied in the terminals, I is the intensity, R_i is the internal resistance of the tachogenerator, W_{FE} is the iron loss, W_{MEC} is the mechanical loss, W_{CU} is the power loss cause by Joule heating, W_{AB} is the power in terminals, N is the rotation speed and K_v is the tachogenerator velocity constant (or back EMF), equal to 1.745 rd/V/s. Basic specifications of the Tachogenerator were extracted from the manufacturer documentation.

The mechanical loss of the tachogenerator as a function of the rotating speed is represented with a solid line in Figure 10.

5.2. Turbine+Tachogenerator loss test

This second test is completed to determine the friction loss of the turbine. The turbine, decoupled from the test bench, is driven by the tachogenerator at different rotating speeds, recording the voltage and the intensity consumed. The difference between the input power and the calculated power loss due to Joule effect is the combined loss of the tachogenerator and the turbine.

Figure 10 also shows the results obtained as a function of the rotating speed (dashed line). As a consequence, the difference between the results obtained in the two former tests allow to obtain the mechanical loss of the turbine.

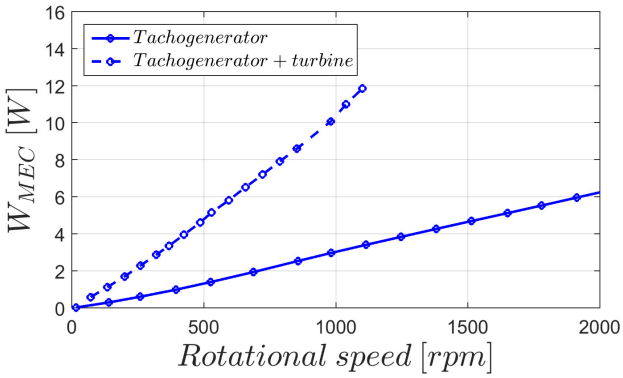

Figure 10.Turbine and tachogenerator mechanical losses

5.3. Turbine test in direct mode

In these tests, when the turbine is working in direct mode with a centrifugal flow (radially outwards), different values of the flow rate coefficient are obtained changing the fan speed for the incoming flow, which makes the turbine to rotate at velocities within the range of 122-1780 rpm.

Under steady conditions, the average values of differential pressure in the Venturi, the inlet static pressure at the inlet and the rotating speed are measured and recorded to determine the input/output power. Note that for this test, the mechanical loss is equal to the torque applied on the turbine blades, so the output power can be extracted from the data obtained in the previous turbine+tachogenerator loss tests. Results for input power against the rotating speed are shown in Figure 11.

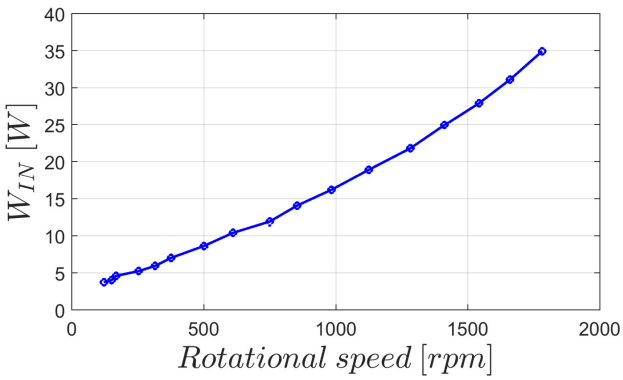

Figure 11. Power input versus rotational speed in direct flow

Taking advantage of the previous tests to characterize the mechanical losses of the facility, the aerodynamic performance of the centrifugal turbine can be finally determined. The results have been obtained in a dimensionless form in Figure 12.

The range of flow coefficients tested, which spreads from 0.6 up to 2.5, is consistent with the typical ranges of flow coefficients found for this type of OWC applications. Moreover, flow coefficients below 0.6 present a sharp drop in efficiency and with small magnitudes of both input and output power so they can be considered negligible for further analysis.

Note that the maximum total-to-static efficiency (right y-axis) reaches values over 50% (in the ϕ = 0.7 range), exceeding by 10% the maximum efficiency reached by previous geometries [18]. This great improvement is achieved due to the blade profile modifications which lead to a significant reduction in kinetic energy loss at the outlet, as previously discussed.

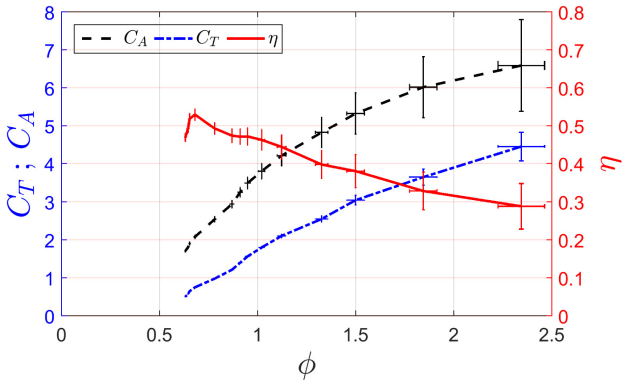

Figure 12. Dimensionless performance in direct mode versus the flow coefficient. Input and torque coefficient, and efficiency in terms of total-to-static. Experimental uncertainty also plot.

Figure 12 also shows both torque and power coefficients with their corresponding uncertainties. In particular, the uncertainty of the flow coefficient is between 0.68% and 5%, whereas the uncertainties of the torque coefficient and the input coefficient are between 0.88% - 8.44% and 2.12% - 18.32% respectively. The efficiency uncertainty is between 2.39% and 20.8%.

5.4. Turbine test in reverse mode

This final test evaluates the performance of the turbine working in the reverse mode. To obtain a centrifugal flow, the duct is now connected to the aspirating region of the fan, while the turbine is driven by the tachogenerator that maintains the rotating speed between 420 and 547 rpm. In addition, the honeycomb is placed at the outlet of the turbine to reduce turbulence and suppress swirls motion, enhancing the Venturi measurement. For every flow rate tested, the following variables are recorded for further post-processing:

static pressure at the outlet of the flow corrector, differential pressure in the Venturi and outlet voltage and current of the tachogenerator. After subtracting the mechanical loss, the performance curves of the turbine on reverse mode are obtained.

The turbine pressure difference with respect the atmospheric condition is measured at the outlet of the flow honeycomb, discounting the honeycomb pressure losses previously assessed. Because the turbine works steadily at equilibrium (the rotating speed is constant), the available output power of the turbine can be measured from the power introduced in the tachogenerator, subtracting the losses by Joule heating, eq. (13), and the tachogenerator + turbine mechanical friction (section 5.2). Finally, the torque is calculated by the expression:

$$T_O = \frac{W_r}{\omega} \qquad Eq.(16)$$

Where W_r is the brake power of the turbine and ω is the rotating speed.

The corresponding flow, torque and input coefficients are then calculated and shown in Figure 13 in dimensionless shape. Note that the torque coefficient is negative, which indicates that the turbine is braking. In this case, the efficiency is meaningless for the analysis so it is not represented here.

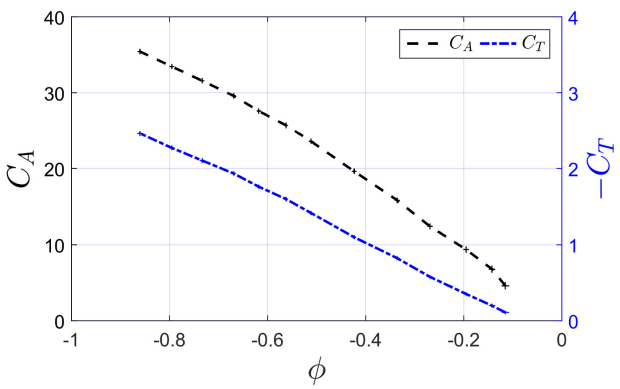

Figure 13. Torque and input dimensionless coefficients versus flow coefficient in reverse mode

The figure also represents the evolution of the power coefficient, including the uncertainties for all the variables. In this case, the uncertainty of the flow coefficient is between 0.5% and 6%. The uncertainty of the torque coefficient is between 1.3% and 16.4% while the uncertainty of the input coefficient is between 0.94% and 9.2%. Note that in these tests, the smaller flow coefficients are achieved by reducing the flow rate, not by a large increase of the rotation speed such as in direct mode tests. This involves that the largest relative uncertainties correspond to the smaller values of the flow coefficient.

The comparison of Figure 12 and Figure 13 reveals the key point of this radial turbine to work in a twin turbine system. The input coefficient in the reverse mode is practically one order of magnitude higher than its value in the direct mode. This means that most of the flow rate generated by the OWC will flow through the turbine working in direct mode because the other turbine, working in reverse mode, will block the flow due to its large amount of loss.

6. Study of the twin turbines system under non-steady conditions

Following, the steady performance results of the turbine are employed to characterize analytically the overall unsteady performance of the twin system, according to the formulation presented in section 2.

The evolution of the instantaneous volumetric efficiency and the direct, reverse and total flow rates in a dimensionless form is obtained over a pressure cycle in Figure 14 for a given flow coefficient of the twin system $\Phi_T = 1.2$ (see Eq. 10).

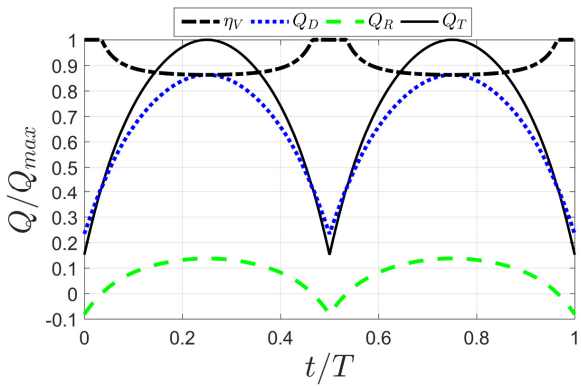

Figure 14. Dimensionless flow Rates and volumetric efficiency under non-steady conditions ($\Phi_T = 1.2$).

The maximum reverse flow rate is 13% of the total flow rate generated within the OWC. Therefore the η_V is, at least, above 87%. This is a remarkable success when it is compared to the usual 60-65% reached by typical axial turbines [15]; and also a significant progress with respect to the 76% of the previous radial geometry [18].

Figure 15 shows the evolution of the efficiencies associated to the non-steady performance of the twin system, defined in eq. (9), as a function of the flowrate coefficient for the system.

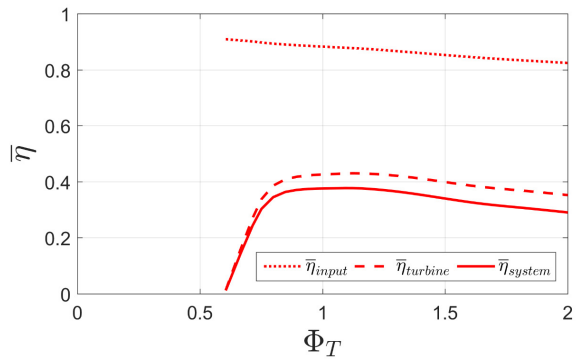

Figure 15. Non-steady efficiency of new twin radial system, and its breakdown terms of turbine efficiency and input efficiency.

The maximum non-steady efficiency reached by the twin turbines is 0.41 for a flow coefficient close to unity. Note that the system efficiency is practically reproducing the efficiency of the turbine due to the extremely high values of the volumetric efficiency. This fact represents the key contribution of this new design of a radial turbine for an OWC application.

7. Results and discussion

In this final section the results obtained for the present investigation are compared to those of the original twin radial turbine [18] and the twin axial turbine referred in [15].

7.1. Steady conditions

Firstly, the results of the new radial turbine are compared in Figure 16 with the quasi-steady performance curve of the twin axial turbine from [15]. There are four basic ideas to be highlighted from the comparison of these steady results:

a) The new radial geometry produces a strong pressure difference in reverse mode which will involve a better performance working as a backflow preventer. This is deduced from the top plot of Figure 16, the ratio between the flow coefficients corresponding to a given C_A, is more favourable in the new geometry.

b) Although the torque in direct mode is being reduced from previous radial geometries (Figure 16, middle plot), it is clear that the efficiency is better due to the reduction of loss. The maximum efficiency, (Figure 16, bottom) is up to 11% better than previous geometries [18].

c) The torque in the reverse mode is neither suppressed nor reduced with respect to the previous radial turbine (Figure 16, middle plot). However, the better performance as a backflow preventer will minimize this effect when working under non-steady conditions.

d) This new radial turbine is more efficient than other radial geometries (Figure 16, bottom) previously published by the authors, for twin systems. Moreover, the reached efficiency gets close to the typical values found for axial geometries [15].

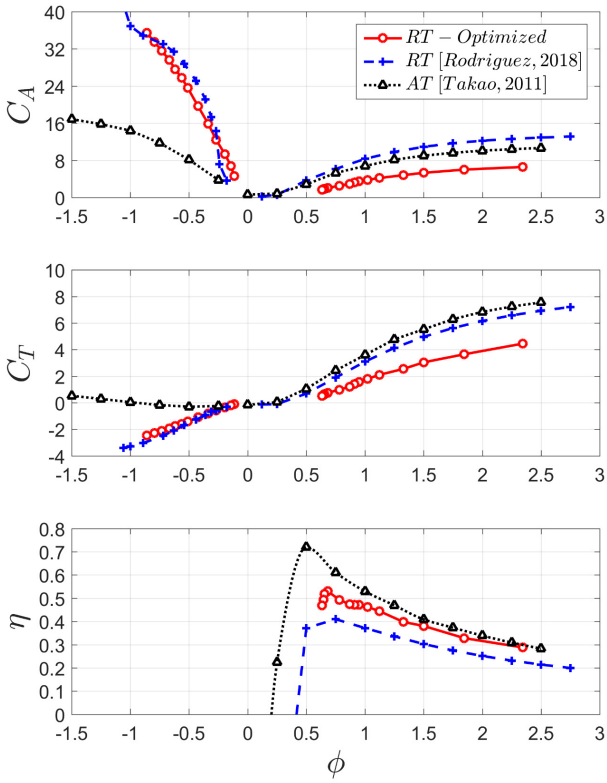

Figure 16. Comparison of stationary performance, Input (top) and torque coefficient (middle), and efficiency (bottom) in terms of total-to-static, with respect to previous geometry and an axial turbine [15].

7.2. Non-steady conditions

In this subsection, the non-steady performance of the twin system is evaluated as a function of the turbine geometry to be installed. Basically, the results of the new radial turbine are shown with respect to the axial turbine extracted from [15] and respect to the original radial turbine taken from [18]. Other geometries have not been included in the graph for a better readability. The three different efficiencies previously defined in eqs. 8-10 for non-steady conditions are represented in Figure 17: the input efficiency $\bar{\eta}_{input}$ on the top, the net efficiency of each turbine $\bar{\eta}_{turbine}$ on the middle and the system efficiency $\bar{\eta}_{system}$ on the bottom.

Looking at the efficiency of the total system, $\bar{\eta}_{system}$ (Figure 17, bottom) the comparison reveals that the new geometry improves the maximum $\bar{\eta}_{system}$ of the previous geometry by a 10%, even the maximum reached by the axial turbine are exceeded by the new radial turbine presented in this work up to 2%. This result could seem surprisingly if only the efficiency of the turbine is taken into account because the efficiency of the axial turbine is larger than the one reached by the radial one, as shown in the bottom plot of Figure 16. However, as it was mentioned before, the system performance under non-steady conditions not only depends on the turbine. The performance working as a backflow preventer, which is critical during the reverse mode, is approximately between 18% an 30% better in case of the new radial turbine with respect to the axial one and 5-10% better than the previous radial geometry from [18]. This implies that a larger part of the flow generated by the OWC is taken in advantage which finally turns into a clear improvement of the system efficiency. Moreover, the improvement of the $\bar{\eta}_{input}$ sparks a side effect: the reverse flow rate is reduced, what involves that the negative torque induced in the turbine working in reverse mode is cut down. Hence, the $\bar{\eta}_{turbine}$ increases, exceeding the maximum $\bar{\eta}_{turbine}$ of the previous turbine by a 11% and closing the gap with respect to axial turbine results.

The results obtained by the new radial geometry endorse the initial idea of the authors that strengthen the performance a backflow preventer was critical in order to improve the system efficiency $\bar{\eta}_{system}$.

Note that, these results, in terms of maximum non-steady efficiencies, can be coarsely compared to those obtained by bidirectional turbines found in [23] and [24] since the analysis technique is similar to the one applied in this work. The maximum non-steady efficiency reached in sinusoidal flow conditions by a bidirectional axial impulse turbine [23] and radial impulse turbine [24] are 39% and 34% respectively. These values are to be compared to the maximum $\bar{\eta}_{system}$ achieved by the twin turbine system, 38% in the case of the new radial turbine presented in this study.

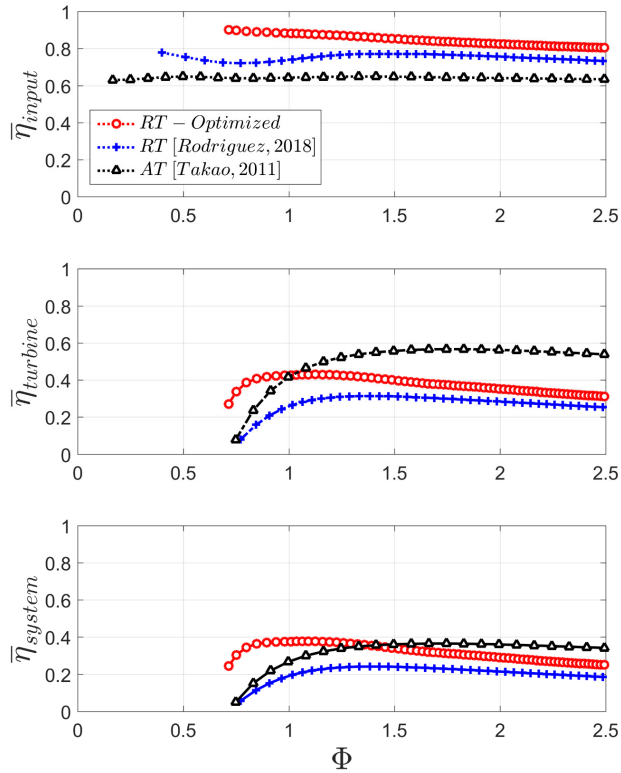

Figure 17. Comparison of non-steady performance, Input efficiency (top) and turbine efficiency (middle), and system efficiency (bottom), with respect to previous geometry and an axial turbine [15].

8. Conclusions

This paper presents the experimental study of an improved design for a radial turbine to be installed in a twin turbine system for an OWC device. The investigation concludes that radial impulse turbine can be a reliable and competitive solution for OWCs equipped with twin turbines system.

The new radial turbine developed for this work includes some geometrical modifications intended to solve both mechanical and aerodynamic problems observed in a previous geometry. In particular, restrictions in the flow circulation that led to significant penalties in the efficiency of the turbine have been now corrected. The experimental results presented confirm the expected improvements and the suitability of the centripetal sense to enhance the performance of the reverse mode. The flow blockage achieved with this configuration is extremely good and it reduces the importance of having negative torque while the air is flowing in centripetal direction because the flow rate is almost negligible in the reverse mode. Definitively, this is the key point that makes radial turbines particularly suitable for twin turbine systems.

Furthermore, the performance in direct mode has been also improved with a redesign of the rotor blades, exhibiting steady efficiencies (total-to-static) close to those obtained by typical axial turbines, supposedly much more efficient. The basic reason for this improvement in the direct mode has been the development of a new blade profile which improves the rotor efficiency and also reduces the kinetic energy loss at the turbine outlet.

All these improvements had led to a clear progress in the performance of twin turbine systems under non-steady conditions, reaching up to a 38% of total system efficiency, which is even higher than previous results obtained by other axial turbines available in the literature. Therefore, radial turbines have demonstrated a definitive potential to be a real solution for twin turbine systems in OWC devices.

9. Acknowledgments

The authors acknowledge the support provided by "Centro Integrado de F.P. Mantenimiento y Servicios a la Producción de Langreo", with special mention to its Director, Mr. F. Fanjul.

10. References:

[1] IPCC. Renewable energy sources and climate change mitigation: special report of the Intergovernmental Panel on Climate Change. Choice Rev Online 2012;49:49-6309-49–6309. doi:10.5860/CHOICE.49-6309.

[2] Falcão AF d. O. Wave energy utilization: A review of the technologies. Renew Sustain Energy Rev 2010;14:899–918. doi:10.1016/j.rser.2009.11.003.

[3] Drew B, Plummer AR, Sahinkaya MN. A review of wave energy converter technology. Proc Inst Mech Eng Part A J Power Energy 2009;223:887–902. doi:10.1243/09576509JPE782.

[4] Palha A, Mendes L, Fortes CJ, Brito-Melo A, Sarmento A. The impact of wave energy farms in the shoreline wave climate: Portuguese pilot zone case study using Pelamis energy wave devices. Renew Energy 2010;35:62–77. doi:10.1016/j.renene.2009.05.025.

[5] Iglesias G, Carballo R. Wave farm impact: The role of farm-to-coast distance. Renew Energy 2014;69:375–85. doi:10.1016/j.renene.2014.03.059.

[6] López I, Andreu J, Ceballos S, Martínez De Alegría I, Kortabarria I. Review of wave energy technologies and the necessary power-equipment. Renew Sustain Energy Rev 2013;27:413–34. doi:10.1016/j.rser.2013.07.009.

[7] Falcão AFO, Henriques JCC. Oscillating-water-column wave energy converters and air turbines: A review. Renew Energy 2016;85:1391–424. doi:10.1016/j.renene.2015.07.086.

[8] Setoguchi T, Takao M. Current status of self rectifying air turbines for wave energy conversion. Energy Convers Manag 2006;47:2382–96. doi:10.1016/j.enconman.2005.11.013.

[9] Falcão AFO, Gato LMC, Henriques JCC, Borges JE, Pereiras B, Castro F. A novel twin-rotor radial-inflow air turbine for oscillating-water-column wave energy converters. Energy 2015;93:2116–25. doi:10.1016/j.energy.2015.10.046.

[10] Wells AA. Rotary transducers. Patent nº US4221538 A, 1980.

[11] Raghunathan S. The wells air turbine for wave energy conversion. Prog Aerosp Sci 1995;31:335–86. doi:10.1016/0376-0421(95)00001-F.

[12] Mala K, Jayaraj J, Jayashankar V, Muruganandam TM, Santhakumar S, Ravindran M, et al. A twin unidirectional impulse turbine topology for OWC based wave energy plants - Experimental validation and scaling. Renew Energy 2011;36:307–14. doi:10.1016/j.renene.2010.06.043.

[13] Jayashankar V, Anand S, Geetha T, Santhakumar S, Jagadeesh Kumar V, Ravindran M, et al. A twin unidirectional impulse turbine topology for OWC based wave energy plants. Renew Energy 2009;34:692–8. doi:10.1016/j.renene.2008.05.028.

[14] Pereiras B, Valdez P, Castro F. Numerical analysis of a unidirectional axial turbine for twin turbine configuration. Appl Ocean Res 2014;47:1–8. doi:10.1016/j.apor.2014.03.003.

[15] Takao M, Takami A, Okuhara S, Setoguchi T. A twin unidirectional impulse turbine for wave energy conversion. J Therm Sci 2011;20:394–7. doi:10.1007/s11630-011-0486-1.

[16] Takao M, Setoguchi T. Air Turbines for Wave Energy Conversion. Int J Rotating Mach 2012;2012:1–10. doi:10.1155/2012/717398.

[17] Pereiras B, Castro F, el Marjani A, Rodríguez MA. Tip Clearance Effect on the Flow Pattern of a Radial Impulse Turbine for Wave Energy Conversion. J Turbomach 2011;133:041019. doi:10.1115/1.4002409.

[18] Rodríguez L, Pereiras B, Fernández-Oro J, Castro F. Viability of unidirectional radial turbines for twin-turbine configuration of OWC wave energy converters. Ocean Eng 2018;154:288–97. doi:10.1016/j.oceaneng.2018.02.010.

[19] Inoue M, Kaneko K, Setoguchi T, Shimamoto K. Studies on Wells Turbine for Wave Power Generator : 4th Report, Starting and Running Characteristics in Periodically Oscillating Flow. Bull

JSME 1986;29:1177–82. doi:10.1299/jsme1958.29.1177.

[20] Hiett GF, Johnston IH. Paper 7: Experiments Concerning the Aerodynamic Performance of Inward Flow Radial Turbines. Proc Inst Mech Eng Conf Proc 1963;178:28–42. doi:10.1243/PIME_CONF_1963_178_214_02.

[21] Thakker A, Khaleeq H Bin, Takao M, Setoguchi T. Effects of hub-to-tip ratio and Reynolds number on the performance of impulse turbine for wave energy power plant. KSME Int J 2003;17:1767–74. doi:10.1007/BF02983607.

[22] Holman JP. Experimental methods for engineers. vol. 9. 1994. doi:10.1016/0894-1777(94)90118-X.

[23] Maeda H, Santhakumar S, Setoguchi T, Takao M, Kaneko K. Performance of impulse turbine with self-pitch-controlled guide vanes for wave power conversion. J Inst Eng Mech Eng Div 2001;82:24–9. doi:10.1016/S0960-1481(98)00771-X.

[24] Pereiras B, Castro F, Marjani A el, Rodríguez MA. An improved radial impulse turbine for OWC. Renew Energy 2011;36:1477–84. doi:10.1016/j.renene.2010.10.013.